



HAL
open science

Enhanced performance of KVPO₄F_{0.5}O_{0.5} in potassium batteries by carbon coating interfaces

Louiza Larbi, Romain Wernert, Philippe Fioux, Laurence Croguennec, Laure Monconduit, Camelia Matei Ghimbeu

► To cite this version:

Louiza Larbi, Romain Wernert, Philippe Fioux, Laurence Croguennec, Laure Monconduit, et al.. Enhanced performance of KVPO₄F_{0.5}O_{0.5} in potassium batteries by carbon coating interfaces. ACS Applied Materials & Interfaces, 2023, 15 (15), pp.18992-19001. 10.1021/acsami.3c01240 . hal-04088055

HAL Id: hal-04088055

<https://hal.science/hal-04088055>

Submitted on 3 May 2023

HAL is a multi-disciplinary open access archive for the deposit and dissemination of scientific research documents, whether they are published or not. The documents may come from teaching and research institutions in France or abroad, or from public or private research centers.

L'archive ouverte pluridisciplinaire **HAL**, est destinée au dépôt et à la diffusion de documents scientifiques de niveau recherche, publiés ou non, émanant des établissements d'enseignement et de recherche français ou étrangers, des laboratoires publics ou privés.

Enhanced performance of $\text{KVPO}_4\text{F}_{0.5}\text{O}_{0.5}$ in potassium batteries by carbon coating interface

Louiza LARBI^{a,b}, Romain WERNERT^{c,d,e}, Philippe FIOUX^{a,b}, Laurence CROGUENNEC^{c, e, f},
Laure MONCONDUIT^{d, e, f}, Camelia MATEI GHIMBEU^{a,b,e,*}

^a Université de Haute-Alsace, Institut de Science des Matériaux de Mulhouse (IS2M), CNRS UMR 7361, F-68100 Mulhouse, France.

^b Université de Strasbourg, F-67081 Strasbourg, France.

^c Université de Bordeaux, CNRS, Bordeaux INP, ICMCB, UMR 5026, F-33600 Pessac, France.

^d ICGM, Université de Montpellier, CNRS, UMR 5253, Montpellier, France.

^e Réseau sur le Stockage Electrochimique de l'Energie, CNRS FR3459, Amiens, France.

^f ALISTORE-European Research Institute, 80039, Amiens, France.

Corresponding author: *E-mail: camelia.ghimbeu@uha.fr

Abstract

Potassium vanadium oxyfluoride phosphate of composition $\text{KVPO}_4\text{F}_{0.5}\text{O}_{0.5}$ was modified by a carbon coating to enhance its electrochemical performance. Two distinct methods were used, first, chemical vapour deposition (CVD) using acetylene gas as carbon precursor and, second, an aqueous route using an abundant, cheap and green precursor (chitosan) followed by a pyrolysis step. The formation of a 5- to 7-nm thick carbon coating was confirmed by transmission electron microscopy (TEM) and it was found to be more homogeneous in the case of CVD using acetylene gas. Indeed, an increase of the specific surface area of one order of magnitude, low content of $\text{C } sp^2$ and residual oxygen surface functionalities were observed when the coating is obtained using chitosan. Pristine and carbon-coated materials were compared as positive electrode materials in potassium half-cells cycled at a $C/5$ ($C = 26.5 \text{ mA g}^{-1}$) rate within the potential window of 3 to 5 V vs K^+/K . The formation by CVD of a uniform carbon coating with the limited presence of surface functions was shown to improve the initial coulombic efficiency (ICE) up to 87% for $\text{KVPFO}_4\text{F}_{0.5}\text{O}_{0.5}\text{-C}_2\text{H}_2$, and to mitigate electrolyte decomposition. Thus, performance at high C rates such as 10C was significantly improved, with ~ 50% of the initial capacity maintained after 10 cycles, whereas a fast capacity loss is observed for the pristine material.

Keywords

Carbon-coating; chemical vapour deposition (CVD); chitosan biopolymer; positive electrode material; vanadium oxyfluoride phosphate; potassium-ion batteries.

1. Introduction

The development of new metal-ion batteries with higher earth abundance and lower cost materials as an alternative to lithium-ion batteries (LIBs) is currently in progress¹. Amongst next-generation batteries, potassium-ion batteries (KIBs) are considered promising candidates for large-scale energy storage. Beside the higher availability of potassium than lithium, KIBs could also allow fast ionic diffusion kinetics of K^+ -ions in the electrolyte, and energy density comparable to LIBs², which can be noticed in the upward spark in publications³. The positive electrode material is obviously critical to achieve a high energy density, high power density, long cycling life, safety, and cost of KIBs⁴.

Various types of materials have been proposed at the positive electrode for KIBs⁵. Among them, we can mention Prussian blue analogues⁶⁻⁹, layered transition metal oxides^{10,11} and polyanionic compounds¹²⁻¹⁴. Phosphate based polyanionic positive electrode materials such as potassium vanadium phosphate fluoride (KVPO₄F) and potassium vanadium phosphate oxide (KVOPO₄) are among the best candidates due to their high theoretical energy density of 560 Wh kg⁻¹, which is similar to that of the commercial LiFePO₄ in LIBs¹⁵⁻¹⁸, and the robustness of their highly covalent framework (promoting high structural and thermal stability)^{15,18,19}. Indeed, KVPO₄F and KVOPO₄ exhibit a theoretical capacity of 131 mAh g⁻¹ (with the exchange of 1 electron (or 1 K⁺) per vanadium) at an average discharge voltage of above 4 V vs K⁺/K. However, they suffer from low electronic conductivity that limits the dynamics of charge transport, increases electrochemical reaction polarisation, and promotes the formation of an unstable electrode/electrolyte interface at high voltages¹⁹⁻²³.

Different methods can be used to solve such issues, and among them, reduction of the particle size, surface modification by carbon coating, or use of carbon-conductive networks^{24,25}. The reduction of particle size to the nanoscale allows a decrease in the ion diffusion length within the solid. However, despite improving the kinetics of the reactions, it also promotes increased

side reactions with the electrolyte due to larger specific surface area, low tap density, and scalable production difficulties²⁵. On the contrary, the formation of carbon coating increases the conductivity using carbon concentrations as low as 0.5-2 wt %, and thus at a low cost and simple preparation²⁶.

Various processes can be used to form a carbon coating, such as thermal spray deposition, physical and chemical vapour deposition (PVD and CVD), electrodeposition (ED) among others^{4,25,27,28}. Carbon surface modified composite materials are also generally prepared by a direct mixing of the active material with a precursor containing carbon (sucrose, glucose...), followed by a heat treatment step^{24,29}. This method allows together to improve the electronic conductivity and to prevent the particle growth and/or aggregation. However, it also leads to a decrease of the tap density and thus of the volumetric capacity. It is worth mentioning that composite preparation can sometimes significantly increase the cost, especially when it requires using carbon nanotubes or graphene to form interconnected conductive networks or adding an additional step in the production line that can be problematic for large-scale production²⁵. However, the formation of carbon coatings is recognized today as an effective way to improve the conductivity and thus the electrochemical performance of different polyanionic positive electrode materials already developed for LIBs and NIBs, despite it has been until now rarely studied for KIBs^{19,20}.

Tian *et al.*²⁴ reported the formation of a carbon coated olivine type LiFePO_4 using glucose as carbon source through a CVD process. The carbon layer as prepared showed high uniformity in coverage and thickness, and as a result led to better electrochemical performance compared to those obtained with conventional coatings prepared by direct mixing (~capacity of ~112 mAh g^{-1} vs ~92 mAh g^{-1} at 100C (1C= 170 mA g^{-1}) and 71% vs. 38% capacity retention at 250C, respectively). Moreover, Lokeswararao *et al.*³⁰, reported the formation of a carbon coating on tavorite LiVPO_4F positive electrode material using lauric acid ($\text{C}_{12}\text{H}_{24}\text{O}_2$) as carbon precursor

and an annealing step. Similarly, the optimized carbon-coated material showed lower polarisation and improved electrochemical performance, in particular at high C-rate (discharge capacity of 44 mAh g⁻¹ at 10C). In addition Fang *et al.*³¹ reported the formation of a carbon coating on NASICON Na₃V₂(PO₄)₃ using C₂H₂ as carbon precursor via a CVD process to create a hierarchical interconnected carbon fibre framework. Higher performance for the coated materials than those of the pristine bare material were successfully obtained in NIBs, i.e., higher capacity, 115 mAh g⁻¹ vs 112 mAh g⁻¹ at 0.2C (C=117 mAh g⁻¹), higher rate capability of 108 mAh g⁻¹ vs 74 mAh g⁻¹ at 10C and 104 mAh g⁻¹ vs 50 mAh g⁻¹ at 20C and better cyclability upon long range cycling.

In addition, the mixture of carbon conductive network such as disorganized carbon (derived from pitch and agarose)^{32,33}, mesoporous carbons³⁴ and carbon nanotubes³⁵ etc, with Na₃V₂(PO₄)₂F₃ and Na₃V₂(PO₄)₃ allow to improve the electrochemical performance of in terms of capacity, rate performance, polar

isation, and cyclability than their initial counter parts. In addition, Liao *et al.* and Liu *et al.* reported recently that electrochemical performance of KVPO₄F in KIBs can be improved significantly by forming a carbon coating and carbon composite^{20,36}. Liao *et al.*^{36,37} prepared a VPO₄ with a flower-like carbon coating which was used as precursor with KF to synthesise a carbon-coated KVPO₄F *via* a multi-step synthesis, isobutanol being the carbon precursor. The modified material showed higher performance than the bare one, i.e., a high capacity of 103 mAh.g⁻¹ at 0.2C and of 87.5 mAh g⁻¹ at 50C (C=100 mA g⁻¹), and long range cycling in KIBs. Liu *et al.*²⁰. proposed KVPO₄F nanoparticles wrapped by an amorphous carbon layer and connected by a 3D carbon conductive network (3DC), this composite material KVPO₄F@3DC was obtained by a soft chemical route and a mechanical activation followed by a low temperature carbonization and calcination process. The as obtained material was tested as a positive electrode in half-cells and showed a high working potential, a discharge capacity of

102 mAh.g⁻¹ vs 98.6 mAh g⁻¹ for the non-coated material at 20 mA g⁻¹, an initial coulombic efficiency (ICE) of 78%, a good cycling stability and a superior rate stability compared to the pristine material. Recently, Liao *et al.* reported a sintering process in which vanadium-oxalate-phosphate is used as vanadium phosphate precursor and template to conserve the plate-like structure and fluorinated polymer PVDF-HFP as fluorine and carbon source to obtain a carbon coated KVPO₄F. The obtained material was tested as positive electrode in K-metal half cell and delivered a capacity of 106 mAh.g⁻¹ vs 94.2 mAh g⁻¹ at 0.2C (C=100 mA g⁻¹). Furthermore, a high rate performance is delivered by the coated material, i.e., 101.3, 97.8 and 93.1 mAh g⁻¹ at 0.5, 20, and 50 C compared to pristine material, i.e., 90.1, 50.2; 22 mAh g⁻¹ at the same C-rates¹⁹.

From the above-mentioned works, it can be summarized that a moderated amount of carbon coating is a key parameter to enhance the electrochemical performance of polyanionic positive electrode materials in different metal ion batteries (LIBs, NIBs and KIBs). Various methods and carbon precursors were used to ensure a homogeneous carbon deposition or composite fabrication. Most of these methods required a multi-steps reactions and are complex to realise, especially for large scale production.

Herein, we propose the formation of a carbon coating for KVPO₄F_{0.5}O_{0.5} positive electrode material which was recently synthesised by a high temperature solid-state reaction described by Wernert *et al.*¹⁶. This material exhibits a specific capacity of 105 mAh.g⁻¹ vs potassium metal, a high working potential of 4.2 V vs K⁺/K and slopping electrochemical curve¹⁶ but also a limited ICE of 80%, and rate capability. Two coating methods, CVD and aqueous route, were used with acetylene and chitosan biopolymer as carbon precursors, respectively. The resulting carbon-coated KVPO₄F_{0.5}O_{0.5} materials present similar crystallographic structures but differ by their surface chemistry and texture. They were evaluated at the positive electrodes in K-metal half cells, and carbon coating has been shown to improve ICE up to 87%, which is among the

highest values for KIB positive electrodes in the literature^{15,16}. Moreover, the rate capability was significantly improved at high C-rates (5 C to 10 C). These remarkable results were explained by the uniform carbon coating, high C sp² content, low specific surface area and small amount of oxygen surface functional groups

2. Experimental

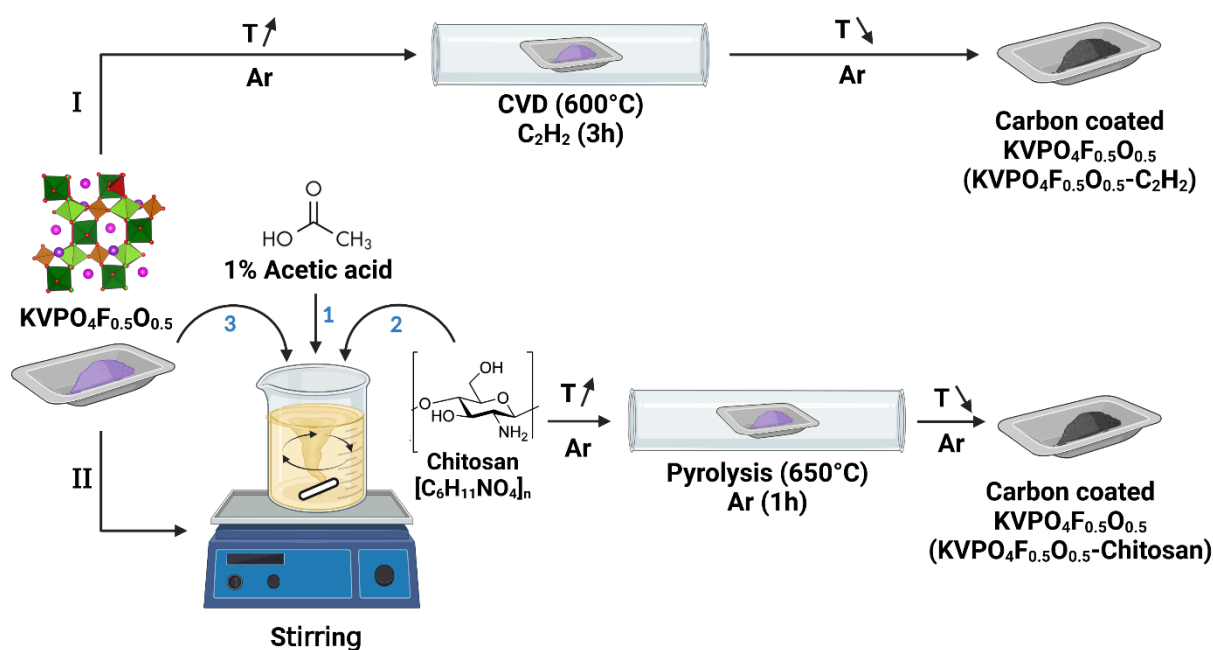
2.1 Material synthesis

KVPO₄F_{0.5}O_{0.5}-C₂H₂ preparation

KVPO₄F_{0.5}O_{0.5} was first synthesized by a solid-state reaction under an argon atmosphere according to previous work reported by some of us¹⁶. The resulting powder was coated with carbon via a CVD process through a thermal decomposition of acetylene (C₂H₂, having a purity of 99.7% vol. abs, purchased from Air Liquide, France) as a carbon precursor in an horizontal furnace as shown in Scheme 1 (I). The sample (700 mg) was placed in a quartz boat and heated under ambient pressure and inert atmosphere (Argon) with a heating rate of 5 °C/min to 600 °C. Then, the Ar flow was stopped, and acetylene was introduced into the system with a flow rate of 1 L/h for 3 hours. Finally, the sample was cooled to room temperature in an inert (argon) atmosphere. This sample is named KVPO₄F_{0.5}O_{0.5}-C₂H₂ in the following.

KVPO₄F_{0.5}O_{0.5}-Chitosan preparation

An aqueous route using Chitosan (Mw = 159.00 g mol⁻¹, Aldrich) as a carbon precursor was used to coat KVPO₄F_{0.5}O_{0.5} material from the same batch as the one used previously to prepare KVPO₄F_{0.5}O_{0.5}-C₂H₂. 120 mg of chitosan was dispersed in 1.5 mL of an aqueous solution of 1% acetic acid, (C₂H₄O₂ Prolabo, 99.8%, 1.05 g cm⁻³ under a strong magnetic stirring, then 750 mg of KVPO₄F_{0.5}O_{0.5} powder was added. The mixture was stirred for 24 hours in an air atmosphere to ensure the homogeneity and the total evaporation of the acetic acid. The material obtained was subsequently pyrolyzed in an argon atmosphere at 650 °C for 1 h with a heating rate of 5 °C min⁻¹, as shown in Scheme 1 (II). The as-obtained material is named KVPO₄F_{0.5}O_{0.5}-Chitosan in the following.



Scheme 1: Schematic representation of the carbon coating synthesis on KVPO₄F_{0.5}O_{0.5} realized by BioRender software: I) coating made by chemical vapour deposition (CVD) with acetylene as carbon precursor and II) coating made by an aqueous solution containing chitosan as carbon precursor followed by pyrolysis.

2.2 Material characterization

The characterisation of the crystalline structure of the materials was performed using X-ray diffraction (XRD), performed on a Bruker D8 ADVANCE A25 diffractometer equipped with a LynxEye XE-T high resolution energy dispersive 1D detector (Cu K $\alpha_{1,2}$), with a flat Bragg-Brentano θ - θ geometry, and operating with a Cu K $\alpha_{1,2}$ X-ray source. XRD patterns were measured in the 10° to 90° 2 θ range with a step size of 0.015° and a counting time of 0.7 s/step. Crystal structure refinement by the Rietveld method was carried out using JANA2006 software.³⁸ A semi-rigid body model was applied to the phosphate groups, allowing the P–O distances to vary between 1.535 ± 0.035 Å.³⁹ Standard uncertainties were corrected using the Bélar-Lelann correction.⁴⁰

Raman spectroscopy was performed to obtain the local structure of the materials using a LabRAM BX40 instrument (Horiba Jobin-Yvon) equipped with a He-Ne excitation source (532 nm wavelength). Nine spectra were acquired per sample by mapping. For a good representativeness of the structure, the average spectrum was used to calculate the I_D/I_G ratio by fitting each band by a Lorentzian function. Furthermore, to probe the distribution, morphology

and crystallinity of the carbon coating, high-resolution transmission electron microscopy (HRTEM) and energy dispersive X-ray spectrometry (EDX) in three distinct zones on the material were performed with a JEOL instrument (ARM-200F model) operating at 200 kV.

Textural characteristics such as specific surface area and pore size distribution were determined with a Micromeritics ASAP 2420 instrument using N₂ adsorbate gas (77 K). The materials were outgazed under vacuum for 12 hours at 150 °C to remove physisorbed molecules. The specific surface area (SSA) was determined based on Brunauer - Emmett - Teller model from the linear plot in the relative pressure range of 0.05 – 0.3 P/P₀. The material pore size distribution (PSD) was obtained by SAIEUS 2.02 software (Micromeritics) using the non-local density functional theory (NLDFT) for a carbon model and standard pore slit.

The carbon amount in the composites was estimated by thermogravimetric analysis (TGA) using a Mettler Toledo instrument. The sample was heated in an alumina (Al₂O₃) crucible under air, from 25 °C to 750 °C at a heating rate of 5 °C min⁻¹. This allows the carbon oxidation and the determination of carbon wt % in the composites based on the mass loss.

The surface chemistry of the coated materials was probed by X-ray photoelectron spectroscopy (XPS) using a SES-2002 (VG SCIENTA) spectrometer equipped by a monochromatic X-ray source (Al K α = 1486.6 eV). Survey and high-resolution spectra were recorded to determine over 5 to 10 nm thickness the nature of the surface functional groups and quantify the amount of carbon coated on the pristine materials.

2.3 Electrochemical Characterisation

2.3.1 Electrode preparation

The working electrodes were prepared by mixing under stirring (900 rpm for 1h) the active material, the polyvinylidene fluoride binder (PVDF from Fluka, M_w = 534 000 g mol⁻¹) and carbon black additive (SuperP from Timcal), with a mass ratio of 80:10:10, in the presence of 1-methyl-2-pyrrolidone solvent (NMP, 99% anhydrous from Sigma Aldrich). The slurry obtained was casted on an aluminium current collector (20 μ m thickness) using the doctor blade method with a blade height of 150 μ m. The resulting film was then dried in air for one night at 80 °C and cut into 16 mm diameter disks with a mass loading of ~ 2.8-3.2 mg cm⁻². The electrodes were uniaxially pressed under 5 t and dried under vacuum for one more night at the same temperature (80 °C), before introducing them in an argon-filled glove box (MBRAUN).

2.3.2 Battery testing conditions

Electrochemical analyses were performed using 316L stainless steel coin cells (CR2032-type) at a controlled room temperature (~ 25 °C) using a multichannel VMP 3 system (BioLogic, France), by assembling several cells for each material to ensure reproducibility of the results.

Coin cells were assembled using electrodes made of $\text{KVPO}_4\text{F}_{0.5}\text{O}_{0.5}$, $\text{KVPO}_4\text{F}_{0.5}\text{O}_{0.5}\text{-C}_2\text{H}_2$, $\text{KVPO}_4\text{F}_{0.5}\text{O}_{0.5}\text{-Chitosan}$ as active materials, two disks of Viledon fiber mat (Freudenberg) as separators (18 mm of diameter), and potassium metal (Alfa Aesar, 99.95%) as a counter electrode (14 mm of diameter). 0.8M of potassium hexafluorophosphate (KPF_6 , from Sigma-Aldrich, $\geq 99\%$) was dissolved in a mixture (50:50 v/v) of ethylene carbonate (EC, from Sigma-Aldrich, $\geq 99\%$) and diethyl carbonate (DEC Sigma-Aldrich, $\geq 99\%$) and used as electrolyte.

Standard galvanostatic tests were performed between 5 and 3 V *vs* K^+/K in half-cells at C/5. The rate performance was evaluated at high C-rates using a standard galvanostatic cycling successfully at C/20, C/10, C/5, C/2, C, 2C, 5C, 10C, respectively. A single cycle was performed at each step (*i.e.* at each C-rate) with a floating time of 2 h at the end of the discharge to ensure that the initial composition ($\text{KVPO}_4\text{F}_{0.5}\text{O}_{0.5}$) was recovered.

3. Results and discussion

3.1 Structure, Texture and Surface properties

Carbon coating was performed on $\text{KVPO}_4\text{F}_{0.5}\text{O}_{0.5}$ positive electrode material with the purpose to improve its electrochemical performance (ICE, rate capability and stability). The choice of this compound was motivated by our previous study¹⁶, which demonstrated that this composition delivers the best performance among those studied in the series of compounds $\text{KVPO}_4\text{F}_{1-y}\text{O}_y$. Indeed, Wernert *et al.*¹⁶ showed that $\text{KVPO}_4\text{F}_{0.5}\text{O}_{0.5}$ behaves better than the end-member composition KVPO_4F , which shows much limited reversibility and cyclability due to a much higher working potential (close to 4.95 V *vs* K^+/K) that leads to huge competition between the K^+ insertion/de-insertion reaction and the irreversible degradation of the electrolyte with a growth of the cathode electrolyte interphase (CEI). Therefore, $\text{KVPO}_4\text{F}_{0.5}\text{O}_{0.5}$ performance is investigated here to be enhanced by modifying its surface by a carbon layer.

The carbon coating deposition on $\text{KVPO}_4\text{F}_{0.5}\text{O}_{0.5}$ was analysed by HRTEM as shown in Figure 1 and Figure S1.

KVPO₄F_{0.5}O_{0.5}-C₂H₂ prepared by CVD process shows a carbon layer around KVPO₄F_{0.5}O_{0.5} particles (Figures S1a-b), while KVPO₄F_{0.5}O_{0.5}-Chitosan made by the aqueous route reveals that carbon is deposited both on and between the particles of KVPO₄F_{0.5}O_{0.5} (Figures S1c-d). Closer inspection by HRTEM allows observing in Figure 1a-b a layer of disorganized carbon for the two kinds of coated samples around KVPO₄F_{0.5}O_{0.5} pristine bare materials, the latter being very organized material as evidenced by the parallel aligned diffraction planes.

KVPO₄F_{0.5}O_{0.5}-Chitosan (Figure 1a), a heterogeneous carbon layer which has different thicknesses between 4 and 10 nm around the pristine material. Differently, for KVPO₄F_{0.5}O_{0.5}-C₂H₂ (Figure 1b), the carbon layer appears better organized and more homogeneous with a constant thickness of around 6 nm than

This was confirmed also by the EDX image of KVPO₄F_{0.5}O_{0.5}-C₂H₂ in Figure 1c which show a homogeneous distribution of carbon (red colour) in and around the particles of the pristine material (other colours). Additional images of the other chemical elements are provided in Figure S2a-f.

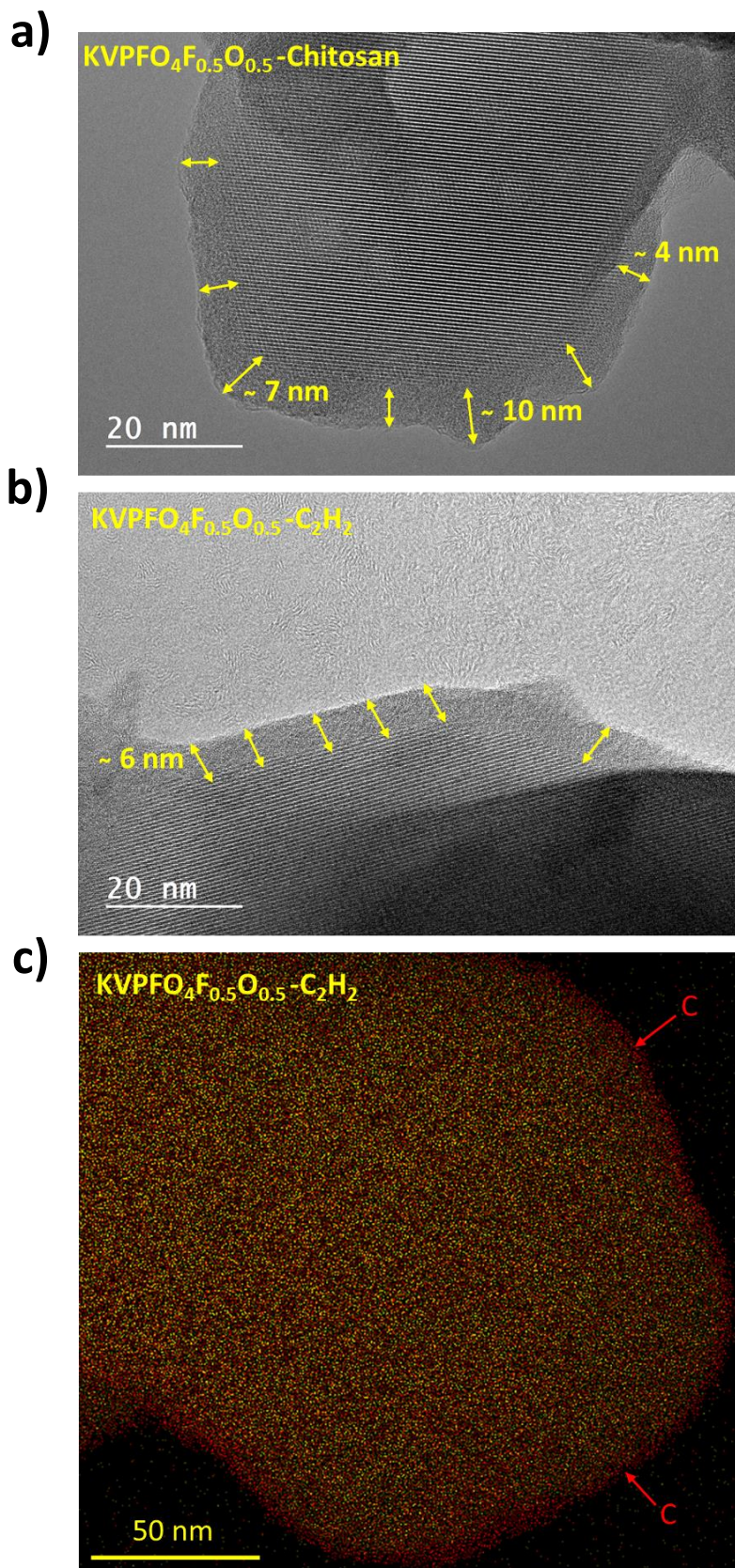


Figure 1: HRTEM images of: (a) $\text{KVPO}_4\text{F}_{0.5}\text{O}_{0.5}$ -Chitosan, (b) $\text{KVPO}_4\text{F}_{0.5}\text{O}_{0.5}$ - C_2H_2 and (c) EDX image of carbon coated $\text{KVPO}_4\text{F}_{0.5}\text{O}_{0.5}$ - C_2H_2 (carbon in red).

The X-ray diffraction analyses of $\text{KVPO}_4\text{F}_{0.5}\text{O}_{0.5}$, $\text{KVPO}_4\text{F}_{0.5}\text{O}_{0.5}\text{-C}_2\text{H}_2$, $\text{KVPO}_4\text{F}_{0.5}\text{O}_{0.5}\text{-Chitosan}$ are shown in Figure 2a. All the samples can be described in an orthorhombic system with the $Pna2_1$ space group. The XRD patterns show that the main crystallographic structure was not influenced by the preparation of the carbon coating, all the samples exhibit the same Bragg peaks before and after the coating formation. Rietveld refinements were performed for the three samples as shown in Figure S3. The cell parameters were found almost identical as witnessed by the unit cell volume of each compound (Table 1). Some small discrepancies in the intensity of the 212 peak were identified, in the order of few percents for the $\text{KVPO}_4\text{F}_{0.5}\text{O}_{0.5}\text{-Chitosan}$ compound, and associated to small K^+ deficiency triggered probably by a cation exchange between K^+ and H^+ in acidic medium (Table S1). Nevertheless, the change is small, and the crystal framework is conserved. For the same material, few very small peaks corresponding either to KVO_3 (due to $\text{KVPO}_4\text{F}_{0.5}\text{O}_{0.5}$ oxidation induced by chitosan) or some unidentified phases have been observed as well.

Raman spectra of the pristine bare and coated materials are shown in Figure 2b. The pristine materials exhibit four distinct bands, at $\sim 520\text{ cm}^{-1}$ corresponding to vanadium-oxygen single bond (V-O)⁴¹, at $\sim 840\text{ cm}^{-1}$ associated to vanadyl bond (V=O)⁴¹, and two bands at $\sim 980\text{ cm}^{-1}$ and 1065 cm^{-1} related to phosphate group (PO_4)⁴². The Raman signatures of the coated samples ($\text{KVPO}_4\text{F}_{0.5}\text{O}_{0.5}\text{-C}_2\text{H}_2$ and $\text{KVPO}_4\text{F}_{0.5}\text{O}_{0.5}\text{-Chitosan}$) show the same bands, with a decrease in absolute intensity for those associated to $\text{KVPO}_4\text{F}_{0.5}\text{O}_{0.5}$ as now its surface is covered by a carbon layer. Furthermore, the coated samples show two additional large bands at $\sim 1300\text{ cm}^{-1}$ and 1600 cm^{-1} , not observed as expected for the bare pristine material, they are well known as the D-band and G-band of carbon⁴³. Generally, the D band is ascribed to the disordered graphite structure whereas the G band reveals the presence of crystallised graphitic carbon^{43,44}. The intensity ratio (I_D/I_G) calculated in Table 1 can be used to estimate the degree of disorder in carbon materials. It is found typical of disordered carbon structure with values of 4.0 for $\text{KVPO}_4\text{F}_{0.5}\text{O}_{0.5}\text{-Chitosan}$ and 3.2 for $\text{KVPO}_4\text{F}_{0.5}\text{O}_{0.5}\text{-C}_2\text{H}_2$ denoting a slightly higher graphitization for the latter. Disordered structures are obtained for these carbon layers as formed at 600-650 °C, which remains rather low for graphitization that starts above 1300 °C.

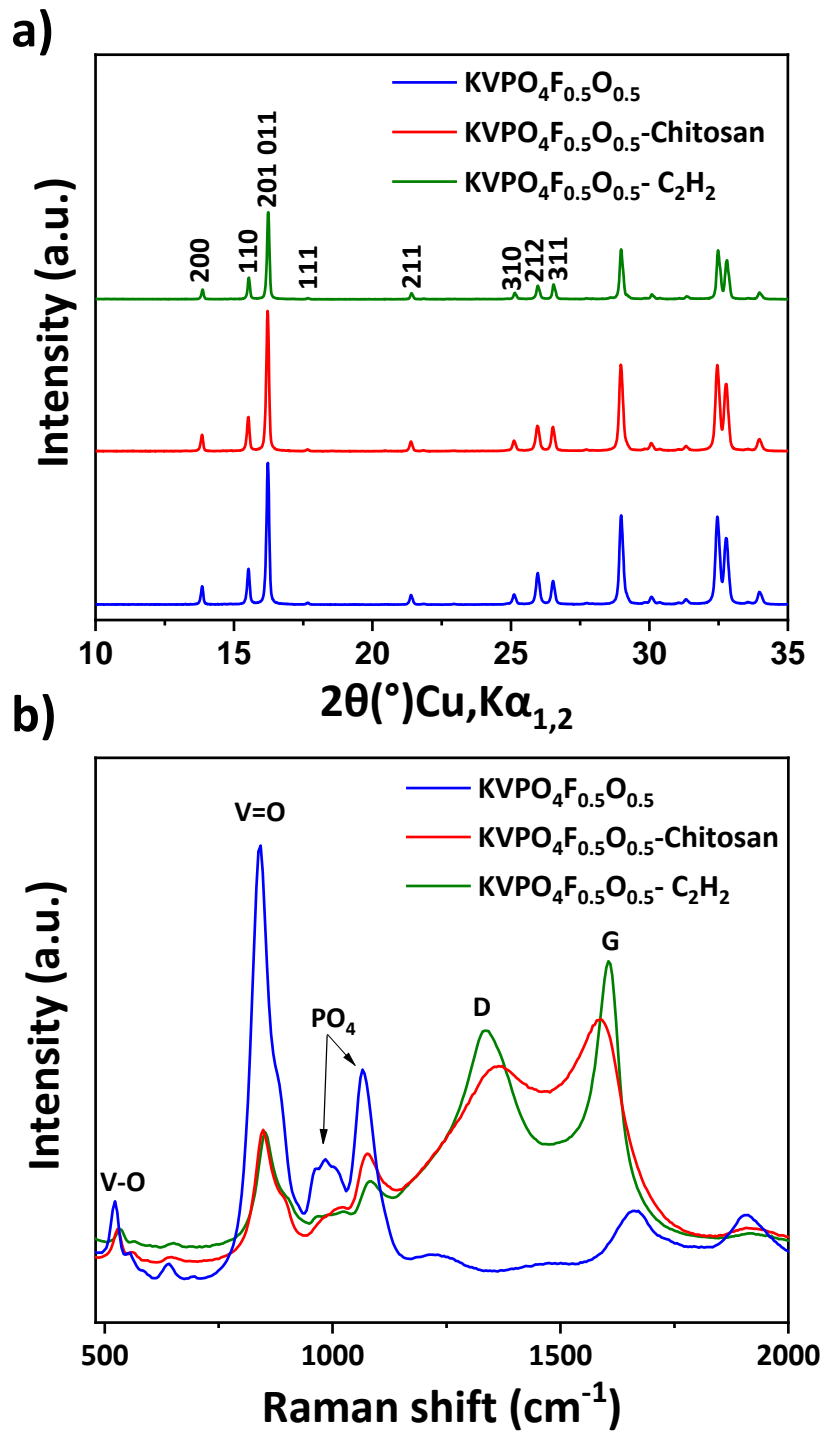


Figure 2: (a) XRD patterns and (b) Raman spectra of KVPO₄F_{0.5}O_{0.5}, KVPO₄F_{0.5}O_{0.5}-Chitosan and KVPO₄F_{0.5}O_{0.5}-C₂H₂.

Table 1: Characteristics of KVPO₄F_{0.5}O_{0.5}, KVPO₄F_{0.5}O_{0.5}-C₂H₂ and KVPO₄F_{0.5}O_{0.5}-Chitosan characteristics including unit cell volume, I_D/I_G, specific surface area (SSA), carbon amount (from TGA) and amount of C1s (from XPS)

Materials	Unit cell volume	I _D /I _G	SSA (m ² g ⁻¹)	C (Wt %), from TGA	C 1s (wt %), from XPS
	V/Z (Å ³)				
KVPO₄F_{0.5}O_{0.5}	107.6 (1) Å ³	N/A	2	N/A	14.3
KVPO₄F_{0.5}O_{0.5}-C₂H₂	107.5 (1) Å ³	3.2	1.3	1	83.1
KVPO₄F_{0.5}O_{0.5}-Chitosan	107.5 (2) Å ³	4.0	17	4	55.2

Textural properties were assessed by N₂ adsorption-desorption isotherms for all materials. As shown in Figure 3a both pristine and KVPO₄F_{0.5}O_{0.5}-C₂H₂ materials show N₂ isotherms of type II, characteristic of low or non-porous materials with an increase of adsorbed volume at P/P₀ ≈ 0.9, which can be due to inter-grains contribution. Pristine material presents a very low specific surface area 2 m²g⁻¹ as reported in Table 1, which is preserved for KVPO₄F_{0.5}O_{0.5}-C₂H₂ (< 2 m² g⁻¹). Such low surface area may favourably influence the electrochemical performance in potassium batteries, by limiting the electrolyte decomposition and the SEI formation.

Differently, KVPO₄F_{0.5}O_{0.5}-Chitosan shows an isotherm of type IV with hysteresis starting at around P/P₀ = 0.45 indicating mesopores capillary condensation behaviour. The BET surface area is also higher (17 m² g⁻¹). Such porosity could be due to the oxygenated groups of the carbon precursor (chitosan) which might induce some gases release during the pyrolysis, enhancing the SSA. The low pyrolysis temperature (650 °C) does not ensure pore closure either⁴⁵.

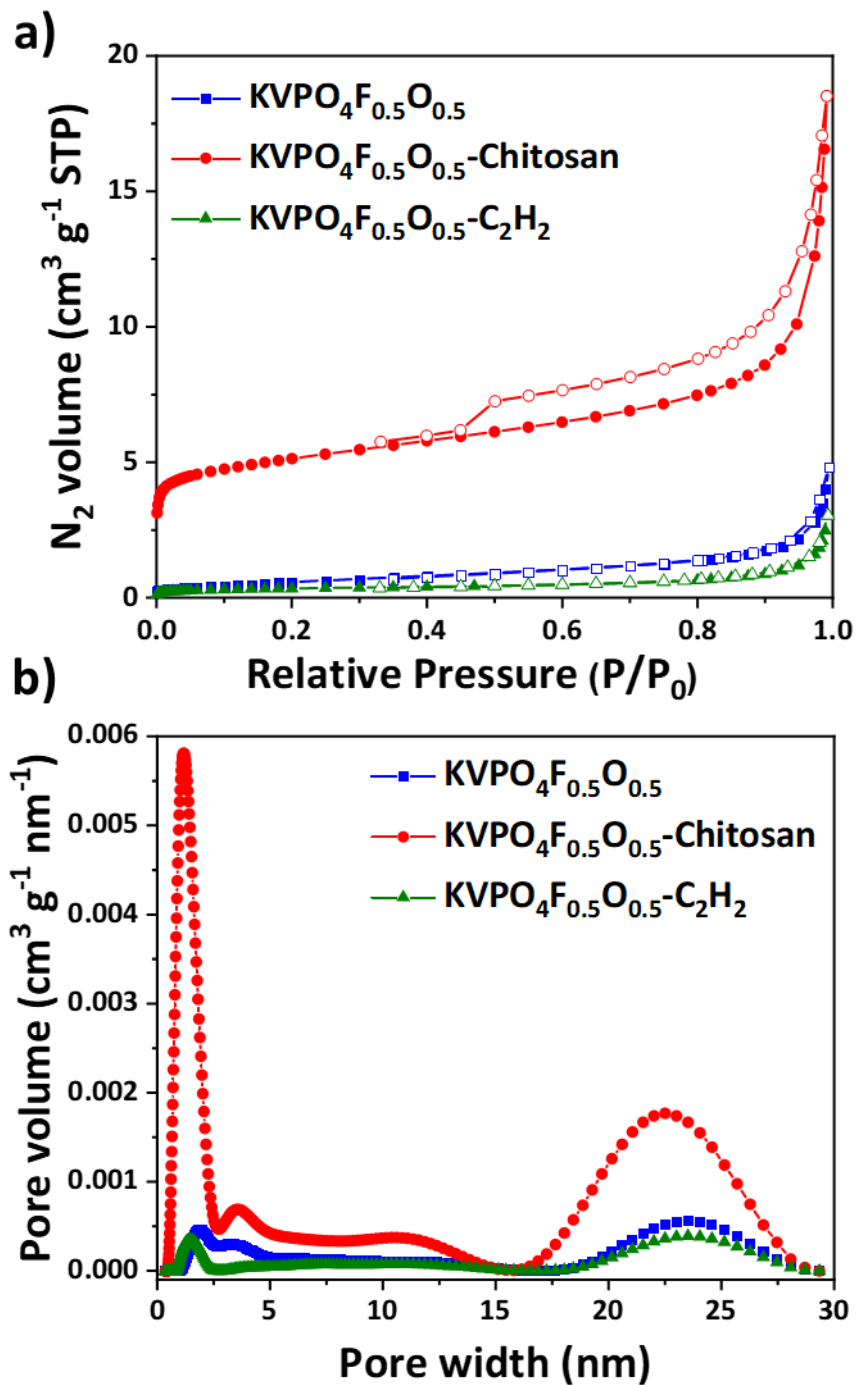


Figure 3: (a) N₂ adsorption - desorption isotherms at 77K and (b) 2D-NLDFT pore size distribution based on N₂ adsorption branch of KVPO₄F_{0.5}O_{0.5}, KVPO₄F_{0.5}O_{0.5}-Chitosan and KVPO₄F_{0.5}O_{0.5}-C₂H₂. Where STP stands for standard conditions of temperature and pressure

Based on the N₂ adsorption results, the pore size distribution of the materials was determined as shown in Figure 3b. Pristine bare KVPO₄F_{0.5}O_{0.5} shows essentially a small volume of micropores with a pore diameter smaller than 2 nm, a small amount of mesopores with pore diameter around 3.5 nm and an important contribution of inter-grains porosity (~17-30 nm). For coated materials, KVPO₄F_{0.5}O_{0.5}-C₂H₂ shows a rather similar pore size distribution as the pristine material, except for the disappearance of the mesopores contribution, while KVPO₄F_{0.5}O_{0.5}-Chitosan reveals a significantly higher amount of micropores (diameter <2 nm), mesopores (3.5 nm) and contribution of inter-grains (~16-30 nm). This significant increase in porosity can be due, as mentioned previously, to much more gases release when chitosan is degraded to form the carbon coating.

Thermogravimetric analysis was carried out under air atmosphere and with a temperature range starting from 25 °C to 750 °C to quantify the amount of carbon deposited at the surface of KVPO₄F_{0.5}O_{0.5} powder. As shown in Figure S4 and Table 1, coated and bare materials were analysed. Bare KVPO₄F_{0.5}O_{0.5} shows a mass gain starting at around 450 °C which can be attributed to its oxidation. For KVPO₄F_{0.5}O_{0.5}-Chitosan the small mass loss of about 1 wt % at a temperature below 100 °C is associated to adsorbed water elimination, it is then followed by a mass loss of 4 wt.% between ~300 to 450 °C which can be attributed to the oxidative pyrolysis of the carbon coating⁴⁶. The same behaviour occurs for KVPO₄F_{0.5}O_{0.5}-C₂H₂ but starting at higher temperature, ~400 °C, and accounts for only 1 wt %⁴⁶. The higher decomposition temperature of acetylene-based coating compared to chitosan-based coating is in good agreement with the formation of a better crystallized carbon layer for the former. As for pristine KVPO₄F_{0.5}O_{0.5}, an increase in the mass is observed for KVPO₄F_{0.5}O_{0.5}-C₂H₂ and KVPO₄F_{0.5}O_{0.5}-Chitosan from ~450 °C range (Figure S4) and attributed to KVPO₄F_{0.5}O_{0.5} oxidation. Lower temperature of oxidation for the coated materials than for the bare material is observed, which might suggest a contribution of carbon in the oxidation process.

Furthermore, XPS was carried out in order to quantify the elements present at the surfaces of KVPO₄F_{0.5}O_{0.5}, with and without carbon coating (Figure S5a-c). KVPO₄F_{0.5}O_{0.5} shows a small contamination with carbon (C1s, mainly C sp³) which can be due to the synthesis conditions. Concerning the coated materials, the C1s intensity peak is lower for KVPO₄F_{0.5}O_{0.5}-Chitosan than for KVPO₄F_{0.5}O_{0.5}-C₂H₂ demonstrating a smaller amount of deposited carbon (C1s) at the surface of the active material particles for the former, *i.e.* 55 at % vs 84 at %, or at least a less homogeneous coverage as shown in Figure S5d.

Other peaks are observed (O1s, K2p, P2s, V2p, V2s, F1s etc.) as shown in Figure S5d. In particular, the O1s peak presents a high intensity in the pristine material (46 at %), which strongly decreases for KVPO₄F_{0.5}O_{0.5}-Chitosan (25 at %) and KVPO₄F_{0.5}O_{0.5}-C₂H₂ (9 at %) while in parallel the C1s peak increases. Similar observations can be done for all the chemical elements contained by KVPO₄F_{0.5}O_{0.5}, *i.e.* K, P, V and F. It supports that the coating with carbon is efficient to cover the extreme surface of KVPO₄F_{0.5}O_{0.5} particles, and that as already mentioned a better coverage is achieved for KVPO₄F_{0.5}O_{0.5}-C₂H₂.

A high amount of carbon and a small amount of oxygen groups on the active material surface may be interesting for better performance as positive electrode materials in KIBs. Indeed, carbon can improve the electronic conductivity of the modified material, whereas a small amount of oxygen may limit the electrolyte decomposition and reduce side reactions between the electrode and electrolyte and, consequently, the SEI formation. To quantify the relative amount of *sp*² and *sp*³ type carbons and oxygen functional groups, the C1s peaks of KVPO₄F_{0.5}O_{0.5}, KVPO₄F_{0.5}O_{0.5}-Chitosan and KVPO₄F_{0.5}O_{0.5}-C₂H₂, have been deconvoluted as shown in Figure 4a-c, allowing their quantification at the surface of the modified powders (Figure 5).

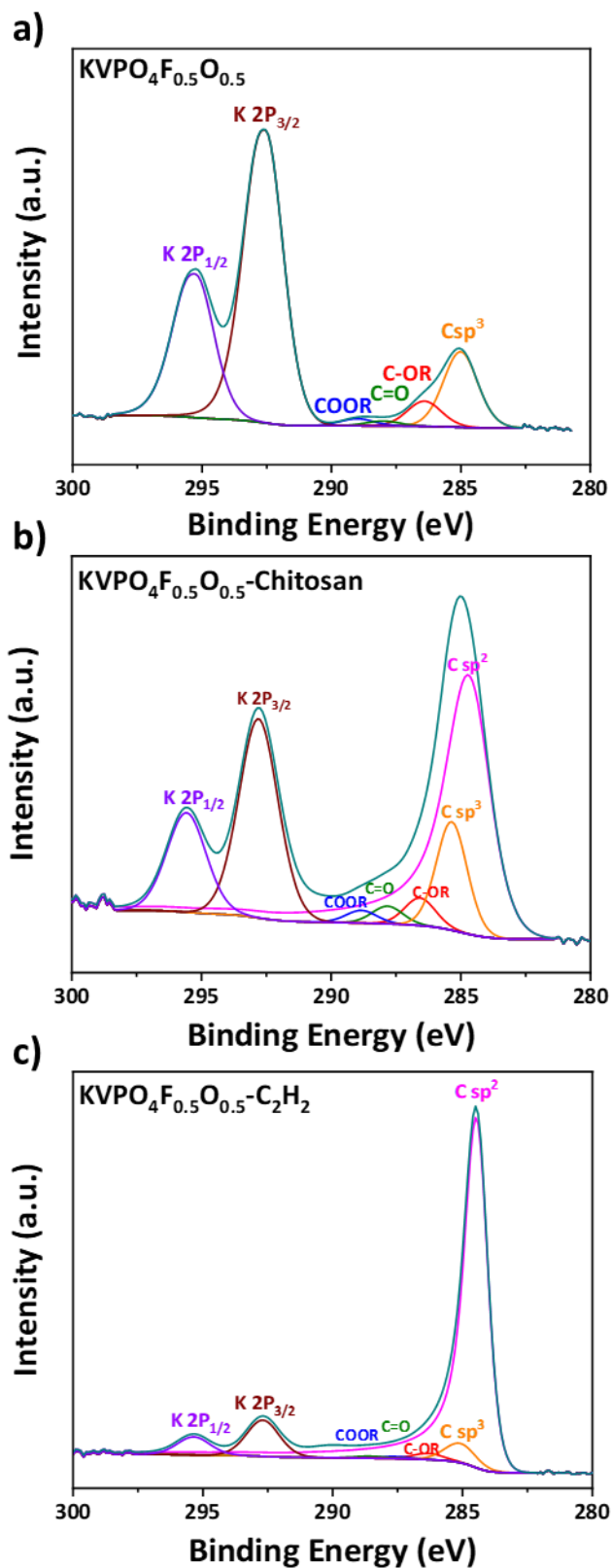


Figure 4: High-resolution C1s XPS spectra of (a) KVPO₄F_{0.5}O_{0.5}, (b) KVPO₄F_{0.5}O_{0.5}-Chitosan and (c) KVPO₄F_{0.5}O_{0.5}-C₂H₂.

The pristine material exhibits mainly sp^3 hybridized carbon associated to oxygenated groups coming from contamination, with K $2p_{3/2}$ and K $2p_{1/2}$ peaks also visible at 292 and 295 eV. For the coated materials, the main contribution comes from conductive sp^2 hybridized carbon (~284 eV). For $KVPO_4F_{0.5}O_{0.5}-C_2H_2$ the C sp^2 peak is very narrow and intense compared to that observed for $KVPO_4F_{0.5}O_{0.5}-Chitosan$. An opposite trend is seen for disordered C sp^3 (285 eV), with a higher relative intensity for $KVPO_4F_{0.5}O_{0.5}-Chitosan$ than for $KVPO_4F_{0.5}O_{0.5}-C_2H_2$. Oxygen-based functional groups are seen as well, at 286 eV (ether, C-OR), 287 eV (carbonyl, C=O) and 289 eV (carboxyl, -COOR)⁴⁷⁻⁴⁹. The amount of these different C sp^3 and oxygen-based chemical species are compared in Figure 5. They are in higher quantity for $KVPO_4F_{0.5}O_{0.5}-Chitosan$ than for $KVPO_4F_{0.5}O_{0.5}-C_2H_2$, in good agreement with the formation of a more disordered carbon for the Chitosan precursor which is richer in oxygen-functional groups than acetylene ($(C_6H_{11}NO_4)_n$ for Chitosan (O/C = 2/3) vs. C_2H_2 for acetylene (O/C = 0)). Moreover, as already discussed in Figure S5d, the intensity of the peaks (K $2p_{3/2}$ and K $2p_{1/2}$) decreased considerably after the formation of the carbon coating, in particular for $KVPO_4F_{0.5}O_{0.5}-C_2H_2$ (Figure 4c), which supports a well-coverage of the material by carbon layer. This material is expected to be more attractive for electrochemical performance.

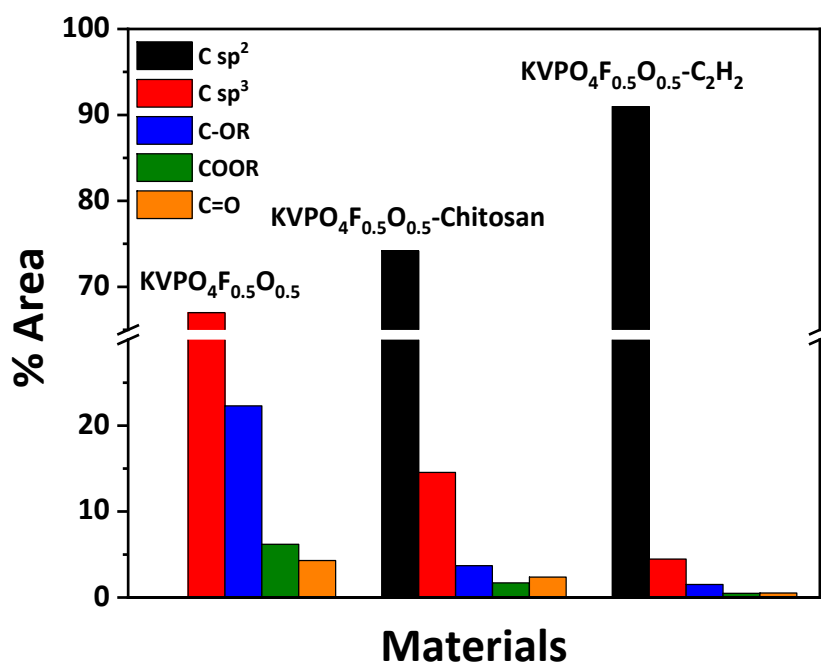


Figure 5: Quantification of chemical species identified from XPS C 1s high-resolution deconvoluted spectra to be present at the surface of $KVPO_4F_{0.5}O_{0.5}$, $KVPO_4F_{0.5}O_{0.5}-C_2H_2$ and $KVPO_4F_{0.5}O_{0.5}-Chitosan$ powder samples.

3.2 Electrochemical performance

The influence of the carbon coating on the electrochemical performance (initial coulombic efficiency, first charge capacity, capacity retention and rate capability) of $\text{KVPO}_4\text{F}_{0.5}\text{O}_{0.5}$ was investigated as shown in Figure 6.

A lower polarisation is observed in the first cycle for coated materials as compared to the pristine bare material. On the other hand, the pristine material exhibits a first charge capacity of 105 mAh g^{-1} and an ICE of 80%, while $\text{KVPO}_4\text{F}_{0.5}\text{O}_{0.5}$ -Chitosan and $\text{KVPO}_4\text{F}_{0.5}\text{O}_{0.5}$ - C_2H_2 show capacities of 87 mAh g^{-1} and 97 mAh g^{-1} and ICE of 83% and 87%, respectively. Therefore, the coated materials exhibit higher ICE compared to that of the bare material, while their capacities are slightly smaller. The improvement of the ICE of carbon-coated materials compared to bare material can be related to the carbon surface poor in oxygen, which limits the decomposition reactions of the electrolyte and the growth of excessive CEI layer, thus providing a more stable electrode / electrolyte interphase (interface). The high conductivity of carbon improves the electrochemical reaction polarisation and allows preservation of high ICE.

In addition, the enhancement of ICE after the formation of carbon coating by the CVD process for $\text{KVPO}_4\text{F}_{0.5}\text{O}_{0.5}$ - C_2H_2 comparing to $\text{KVPO}_4\text{F}_{0.5}\text{O}_{0.5}$ -Chitosan can be explained by i) the better coverage of the $\text{KVPO}_4\text{F}_{0.5}\text{O}_{0.5}$ surface, ii) the higher content of hybridized carbon sp^2 as demonstrated by XPS, iii) the lower amount of oxygen-based functional groups and iv) the lower SSA compared to chitosan-coated material.

Furthermore, cycling performance evaluation of $\text{KVPO}_4\text{F}_{0.5}\text{O}_{0.5}$ - C_2H_2 was done at C/5 (3 - 5 V vs. K^+/K) as seen in Figure 6c. It presents a capacity retention of 88% at the 20th cycle, which shows that the coated sample exhibits cyclability which is in the same range as KVPO_4F studied in literature by Kim *et al.* and Chihara *et al.*^{18,22}. The three materials were tested at different C-rates (Figure 6d), both carbon coated materials show a rather similar behaviour than the pristine bare material at low C rates ($< 2\text{C}$), with a decrease in capacity of $\sim 40\%$ for the pristine material, $\sim 34\%$ for $\text{KVPO}_4\text{F}_{0.5}\text{O}_{0.5}$ -Chitosan and 29% for $\text{KVPO}_4\text{F}_{0.5}\text{O}_{0.5}$ - C_2H_2 . At higher C-rates ($> 2\text{C}$), the pristine material exhibits a severe capacity drop and is for instance not able to provide any capacity at 10C , while the coated materials $\text{KVPO}_4\text{F}_{0.5}\text{O}_{0.5}$ -Chitosan and $\text{KVPO}_4\text{F}_{0.5}\text{O}_{0.5}$ - C_2H_2 preserve 48% and 54% of their initial capacity, respectively. This difference in terms of rate capability between carbon coated and bare materials can be explained by the increasing difficulty to couple transport of ions and electrons as the C-rate increases. The formation of conductive composites helps to maintain high-rate performance by improving the

collection and transport of the electrons, and thus of the ions within the bulk of the electrode. This strategy is shown to be successful in Figure 6d as for the bare material the capacity decreases continuously due to ionic diffusion limitation up to 2C and then abruptly above 2C due to strong electronic transport limitation, whereas for the carbon coated materials a smooth, continuous and limited decrease in capacity is observed over the same range of C-rates explored.

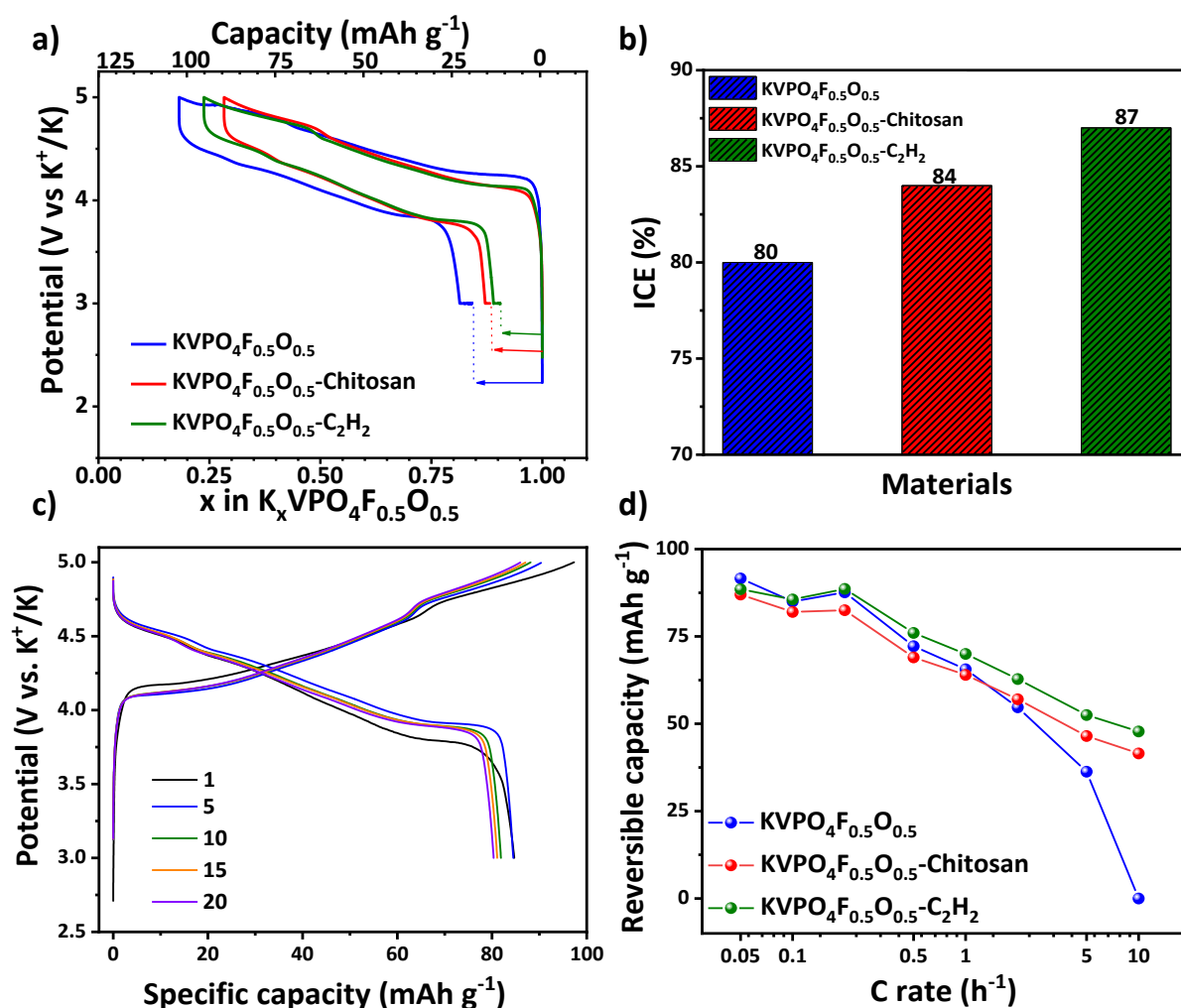


Figure 6: (a) First charge-discharge cycle at C/5; (b) initial coulombic efficiency; (c) comparison of different charge and discharge curves for KVPO₄F_{0.5}O_{0.5}-C₂H₂ at C/5 (1st, 5th, 10th, 15th and 20th cycles); (d) Reversible discharge capacity at different C-rates for KVPO₄F_{0.5}O_{0.5}, KVPO₄F_{0.5}O_{0.5}-Chitosan and KVPO₄F_{0.5}O_{0.5}-C₂H₂.

Table 2 gives a comparison between the electrochemical performance obtained for potassiated vanadium phosphates in the frame of this work and others reported in literature. It appears that

the ICE obtained for KVPO₄F_{0.5}O_{0.5}-Chitosan and KVPO₄F_{0.5}O_{0.5}-C₂H₂ samples are among the highest values reported in literature, with acceptable charge and discharge capacities. Moreover, KVPO₄F_{0.5}O_{0.5}-C₂H₂ presents a good capacity retention of 88% after the 20th cycle at C/5.

Table 2: Comparison of electrochemical performance reported for different KIB positive electrode materials.

Material	Electrolyte	Average voltage (V)	Discharge capacity (mAh g ⁻¹)	Charge capacity (mAh g ⁻¹)	ICE (%)	Capacity retention (%)	Reference
KVPO₄F	0.7 M KPF ₆ / EC:DEC (1:1 v/v)	4.1	~80	~170	~50	97 (30 cycles)	18
KVOPO₄	0.7 M KPF ₆ / EC:DEC (1:1 v/v)	4.1	~80	~175	<50	97 (30 cycles)	
KVPO₄F	0.7 M KPF ₆ / EC:DEC (1:1 v/v)	4.0	~70	~160	<50	90.7 (compared to 2 nd cycle)	
KVOPO₄	0.7 M KPF ₆ / EC:DEC (1:1 v/v)	3.9	~70	~140	<50	93.9 (compared to 2 nd cycle)	
KVPO₄F_{0.5}O_{0.5}	0.8 M KPF ₆ / EC:DEC (1:1 v/v)	4.2	84	105	80	N/A	16
KVPO₄F	0.7 M KPF ₆ / EC:DEC (1:1 v/v)	4.1	~140	~95	~ 67	~87 (30 cycles) ~47 (200 cycles)	22
KVPO₄F@3DC	0.8 M KPF ₆ / EC:DEC (1:1 v/v)	4.1	104.4	130	80	83.6 (100 cycles)	20
KVPO₄F/C	1 M KPF ₆ / EC:PC (1:1 v/v)	4.2	~138	106	~76	N/A	19
KVPO₄F	0.8 M KPF ₆ / EC:DEC (50:50 v/v)	4.3	N/A	N/A	N/A	62 (70 cycles)	21

KVPO₄F-C	0.8 M KPF ₆ / EC:DEC (50:50 v/v)	4.3	N/A	N/A	N/A	76 (70 cycles)	
K-MnHCFe	0.7M KPF ₆ / EC:DEC (1:1 v/v)	3.5	60	110	~54	~80 (60 cycles)	50
KVPO₄F_{0.5}O_{0.5}- C₂H₂	0.8 M KPF ₆ / EC:DEC (50:50 v/v)	4.2	84	97	87	88 (20 cycles)	This work

Conclusion

The influence of a carbon coating on KVPO₄F_{0.5}O_{0.5} used as positive electrode material in KIBs was addressed. Two different methods, CVD from C₂H₂ and chitosan in aqueous media followed by a pyrolysis step, were explored to perform the carbon coating. Neither the morphology nor the crystallographic structure of KVPO₄F_{0.5}O_{0.5} were affected by the coating process, while SSA increased considerably for KVPFO₄F_{0.5}O_{0.5}-Chitosan. In fact, the deposited carbon layer was found to be more homogeneous, in thickness and in coverage, and crystallized for KVPFO₄F_{0.5}O_{0.5}-C₂H₂. Indeed, the amount of carbon sp² was revealed to be higher and of oxygen functional groups to be lower for KVPFO₄F_{0.5}O_{0.5}-C₂H₂ compared to KVPFO₄F_{0.5}O_{0.5}-Chitosan. Carbon coated materials showed improved electrochemical performance with ICE up to 87% for KVPFO₄F_{0.5}O_{0.5}-C₂H₂ versus 80% for the bare pristine material, those ICE being among the highest values reported in the literature. Additionally, the carbon coating allows improving cycling performance and rate capability with the retention of ~50% of the initial capacity at a high rate of 10C, compared to almost 0% for pristine bare material. This improvement brought by the surface modification of the active material KVPO₄F_{0.5}O_{0.5} by an homogeneous carbon layer is likely due to both, the increase of the KVPO₄F_{0.5}O_{0.5} composite electrode conductivity, and the limitation of side reactions at the interface between the active material and the electrolyte which is highly critical for this new-born KIB technology as the electrolytes still require to be optimized. An extended XPS study upon cycling is in progress in order to determine the impact of the coating on the nature and amount of species building the SEI with the carbon coated and bare KVPO₄F_{0.5}O_{0.5} samples.

Conflict of Interest

The authors declare no conflict of interest.

Supporting Information:

TEM images of the carbon coated $\text{KVPO}_4\text{F}_{0.5}\text{O}_{0.5}$ at different scales; EDX images of the elemental composition of $\text{KVPO}_4\text{F}_{0.5}\text{O}_{0.5}\text{-C}_2\text{H}_2$ material; Rietveld refinements of the XRD patterns of the bare and carbon coated $\text{KVPO}_4\text{F}_{0.5}\text{O}_{0.5}$ materials; cell parameters and K^+ site occupancy refined by the Rietveld method for all the materials; TGA curves of all materials; XPS wide scan and atomic percentages of elements at the surface of the bare and the coated materials.

Acknowledgements

LL and RW PhD grants were funded by the Algerian Ministry of High Education and Scientific Research and Agence Nationale de la Recherche, respectively. The authors acknowledge financial support of the Agence Nationale de la Recherche (ANR) under Grants ANR-19-CE05-0026 (TROPIC project) and ANR-10-LABX-76-01 (RS2E (French research network on electrochemical energy storage), STORE-EX Labex Project), as well as Région Nouvelle Aquitaine for sustaining this work.

The authors thank the technical staff of “Carbon and Hybrid Material” team (Adrian Beda, Joseph Dentzer and Bénédicte Réty) for their daily support with the fabrication and analyses of carbon materials. The authors thank Dr. Loïc Vidal (HRTEM images), Dr. Jean-Marc Le Meins (XRD data) and Dr. Cyril Vaultot (gas adsorption) for technical support via IS2M technical platforms. The authors thank the technical staff of ICGM and ICMCB for their experimental help.

References

- (1) Eftekhari, A.; Jian, Z.; Ji, X. Potassium Secondary Batteries. *ACS Appl. Mater. Interfaces* **2017**, *9* (5), 4404–4419. <https://doi.org/10.1021/acsami.6b07989>.
- (2) Zhang, W.; Mao, J.; Li, S.; Chen, Z.; Guo, Z. Phosphorus-Based Alloy Materials for Advanced Potassium-Ion Battery Anode. *J. Am. Chem. Soc.* **6**.
- (3) Ahmed, S. M.; Suo, G.; Wang, W. A.; Xi, K.; Iqbal, S. B. Improvement in Potassium Ion Batteries Electrodes: Recent Developments and Efficient Approaches. *J. Energy Chem.* **2021**, *62*, 307–337. <https://doi.org/10.1016/j.jechem.2021.03.032>.
- (4) Zhang, Q.; Wang, Z.; Zhang, S.; Zhou, T.; Mao, J.; Guo, Z. Cathode Materials for Potassium-Ion Batteries: Current Status and Perspective. *Electrochem. Energy Rev.* **2018**, *1* (4), 625–658. <https://doi.org/10.1007/s41918-018-0023-y>.

- (5) Li, P.; Kim, H.; Kim, K.-H.; Kim, J.; Jung, H.-G.; Sun, Y.-K. State-of-the-Art Anodes of Potassium-Ion Batteries: Synthesis, Chemistry, and Applications. *Chem. Sci.* **2021**, *12* (22), 7623–7655. <https://doi.org/10.1039/D0SC06894B>.
- (6) Su, D.; McDonagh, A.; Qiao, S.; Wang, G. High-Capacity Aqueous Potassium-Ion Batteries for Large-Scale Energy Storage. *Adv. Mater.* **2017**, *29* (1), 1604007. <https://doi.org/10.1002/adma.201604007>.
- (7) Wang, B.; Han, Y.; Wang, X.; Bahlawane, N.; Pan, H.; Yan, M.; Jiang, Y. Prussian Blue Analogs for Rechargeable Batteries. *iScience* **2018**, *3*, 110–133. <https://doi.org/10.1016/j.isci.2018.04.008>.
- (8) Zhou, A.; Cheng, W.; Wang, W.; Zhao, Q.; Xie, J.; Zhang, W.; Gao, H.; Xue, L.; Li, J. Hexacyanoferrate-Type Prussian Blue Analogs: Principles and Advances Toward High-Performance Sodium and Potassium Ion Batteries. *Adv. Energy Mater.* **2021**, *11* (2), 2000943. <https://doi.org/10.1002/aenm.202000943>.
- (9) Hurlbutt, K.; Wheeler, S.; Capone, I.; Pasta, M. Prussian Blue Analogs as Battery Materials. *Joule* **2018**, *2* (10), 1950–1960. <https://doi.org/10.1016/j.joule.2018.07.017>.
- (10) Hironaka, Y.; Kubota, K.; Komaba, S. P2- and P3-K_xCoO₂ as an Electrochemical Potassium Intercalation Host. *Chem. Commun.* **2017**, *53* (26), 3693–3696. <https://doi.org/10.1039/C7CC00806F>.
- (11) Nathan, M. G. T.; Yu, H.; Kim, G.-T.; Kim, J.-H.; Cho, J. S.; Kim, J.; Kim, J.-K. Recent Advances in Layered Metal-Oxide Cathodes for Application in Potassium-Ion Batteries. *Adv. Sci.* **2022**, *9* (18), 2105882. <https://doi.org/10.1002/advs.202105882>.
- (12) Recham, N.; Rousse, G.; Sougrati, M. T.; Chotard, J.-N.; Frayret, C.; Mariyappan, S.; Melot, B. C.; Jumas, J.-C.; Tarascon, J.-M. Preparation and Characterization of a Stable FeSO₄F-Based Framework for Alkali Ion Insertion Electrodes. *Chem. Mater.* **2012**, *24* (22), 4363–4370. <https://doi.org/10.1021/cm302428w>.
- (13) Hosaka, T.; Shimamura, T.; Kubota, K.; Komaba, S. Polyanionic Compounds for Potassium-Ion Batteries. *Chem. Rec.* **2019**, *19* (4), 735–745. <https://doi.org/10.1002/tcr.201800143>.
- (14) Hosaka, T.; Kubota, K.; Hameed, A. S.; Komaba, S. Research Development on K-Ion Batteries. *Chem. Rev.* **2020**, *acs.chemrev.9b00463*. <https://doi.org/10.1021/acs.chemrev.9b00463>.
- (15) Kim, H.; Seo, D.-H.; Bianchini, M.; Clément, R. J.; Kim, H.; Kim, J. C.; Tian, Y.; Shi, T.; Yoon, W.-S.; Ceder, G. A New Strategy for High-Voltage Cathodes for K-Ion Batteries:

- Stoichiometric KVPO₄F. *Adv. Energy Mater.* **2018**, *8* (26), 1801591. <https://doi.org/10.1002/aenm.201801591>.
- (16) Wernert, R.; Nguyen, L. H. B.; Petit, E.; Camacho, P. S.; Iadecola, A.; Longo, A.; Fauth, F.; Stievano, L.; Monconduit, L.; Carlier, D.; Croguennec, L. Controlling the Cathodic Potential of KVPO₄F through Oxygen Substitution. *Chem. Mater.* **2022**, *34* (10), 4523–4535. <https://doi.org/10.1021/acs.chemmater.2c00295>.
- (17) Masquelier, C.; Croguennec, L. Polyanionic (Phosphates, Silicates, Sulfates) Frameworks as Electrode Materials for Rechargeable Li (or Na) Batteries. *Chem. Rev.* **2013**, *113* (8), 6552–6591. <https://doi.org/10.1021/cr3001862>.
- (18) Chihara, K.; Katogi, A.; Kubota, K.; Komaba, S. KVPO₄F and KVOPO₄ toward 4 Volt-Class Potassium-Ion Batteries. *Chem. Commun.* **2017**, *53* (37), 5208–5211. <https://doi.org/10.1039/C6CC10280H>.
- (19) Liao, J.; Zhang, X.; Zhang, Q.; Hu, Q.; Li, Y.; Du, Y.; Xu, J.; Gu, L.; Zhou, X. Synthesis of KVPO₄F/Carbon Porous Single Crystalline Nanoplates for High-Rate Potassium-Ion Batteries. *Nano Lett.* **2022**, *22* (12), 4933–4940. <https://doi.org/10.1021/acs.nanolett.2c01604>.
- (20) Liu, Z.; Wang, J.; Lu, B. Plum Pudding Model Inspired KVPO₄F@3DC as High-Voltage and Hyperstable Cathode for Potassium Ion Batteries. *Sci. Bull.* **2020**, *65* (15), 1242–1251. <https://doi.org/10.1016/j.scib.2020.04.010>.
- (21) Caracciolo, L.; Madec, L.; Petit, E.; Gabaudan, V.; Carlier, D.; Croguennec, L.; Martinez, H. Electrochemical Redox Processes Involved in Carbon-Coated KVPO₄F for High Voltage K-Ion Batteries Revealed by XPS Analysis. *J. Electrochem. Soc.* **2020**, *167* (13), 130527. <https://doi.org/10.1149/1945-7111/abbb0c>.
- (22) Kim, H.; Tian, Y.; Ceder, G. Origin of Capacity Degradation of High-Voltage KVPO₄F Cathode. *J. Electrochem. Soc.* **2020**, *167* (11), 110555. <https://doi.org/10.1149/1945-7111/aba54e>.
- (23) Wernert, R.; Nguyen, L. H. B.; Iadecola, A.; Weill, F.; Fauth, F.; Monconduit, L.; Carlier, D.; Croguennec, L. Self-Discharge Mechanism of High-Voltage KVPO₄F for K-Ion Batteries. *ACS Appl. Energy Mater.* **2022**, *5* (12), 14913–14921. <https://doi.org/10.1021/acsaem.2c02379>.
- (24) Tian, R.; Liu, H.; Jiang, Y.; Chen, J.; Tan, X.; Liu, G.; Zhang, L.; Gu, X.; Guo, Y.; Wang, H.; Sun, L.; Chu, W. Drastically Enhanced High-Rate Performance of Carbon-Coated LiFePO₄ Nanorods Using a Green Chemical Vapor Deposition (CVD) Method for

- Lithium Ion Battery: A Selective Carbon Coating Process. *ACS Appl. Mater. Interfaces* **2015**, 7 (21), 11377–11386. <https://doi.org/10.1021/acsami.5b01891>.
- (25) Zhang, Z.; Wang, R.; Chen, Z.; Liu, X.; Liu, Z.; Zeng, J.; Zhao, X.; Peng, K.; Yao, Q.; Zhang, X.; Shi, K.; Zhu, C.; Yan, X. A Micron-Size Carbon-Free $\text{K}_3\text{V}_2\text{O}_2(\text{PO}_4)_2\text{F}$ Cathode with High-Rate Performance for Potassium-Ion Batteries. *Chem. Eng. J.* **2022**, 436, 135235. <https://doi.org/10.1016/j.cej.2022.135235>.
- (26) Wang, J.; Sun, X. Understanding and Recent Development of Carbon Coating on LiFePO_4 Cathode Materials for Lithium-Ion Batteries. *Energy Env. Sci* **2012**, 5 (1), 5163–5185. <https://doi.org/10.1039/C1EE01263K>.
- (27) Wang, F.; Song, X.; Yao, G.; Zhao, M.; Liu, R.; Xu, M.; Sun, Z. Carbon-Coated Mesoporous SnO_2 Nanospheres as Anode Material for Lithium Ion Batteries. *Scr. Mater.* **2012**, 66 (8), 562–565. <https://doi.org/10.1016/j.scriptamat.2012.01.003>.
- (28) Tyagi, A.; Walia, R. S.; Murtaza, Q.; Pandey, S. M.; Tyagi, P. K.; Bajaj, B. A Critical Review of Diamond like Carbon Coating for Wear Resistance Applications. *Int. J. Refract. Met. Hard Mater.* **2019**, 78, 107–122. <https://doi.org/10.1016/j.ijrmhm.2018.09.006>.
- (29) Kadoma, Y.; Kim, J.-M.; Abiko, K.; Ohtsuki, K.; Ui, K.; Kumagai, N. Optimization of Electrochemical Properties of LiFePO_4/C Prepared by an Aqueous Solution Method Using Sucrose. *Electrochimica Acta* **2010**, 55 (3), 1034–1041. <https://doi.org/10.1016/j.electacta.2009.09.029>.
- (30) Lokeswararao, Y.; Sudarshan, C.; Sudakar, C. Optimizing Carbon Coating to Synthesize Phase Pure LiVPO_4F Cathode through a Combined Sol-Gel and PTFE Reaction. *Mater. Chem. Phys.* **2021**, 263, 124362. <https://doi.org/10.1016/j.matchemphys.2021.124362>.
- (31) Fang, Y.; Xiao, L.; Ai, X.; Cao, Y.; Yang, H. Hierarchical Carbon Framework Wrapped $\text{Na}_3\text{V}_2(\text{PO}_4)_3$ as a Superior High-Rate and Extended Lifespan Cathode for Sodium-Ion Batteries. *Adv. Mater.* **2015**, 27 (39), 5895–5900. <https://doi.org/10.1002/adma.201502018>.
- (32) Wang, M.; Huang, X.; Wang, H.; Zhou, T.; Xie, H.; Ren, Y. Synthesis and Electrochemical Performances of $\text{Na}_3\text{V}_2(\text{PO}_4)_2\text{F}_3/\text{C}$ Composites as Cathode Materials for Sodium Ion Batteries. *RSC Adv.* **2019**, 9 (53), 30628–30636. <https://doi.org/10.1039/C9RA05089B>.
- (33) Gu, Z.-Y.; Guo, J.-Z.; Sun, Z.-H.; Zhao, X.-X.; Li, W.-H.; Yang, X.; Liang, H.-J.; Zhao, C.-D.; Wu, X.-L. Carbon-Coating-Increased Working Voltage and Energy Density towards an Advanced $\text{Na}_3\text{V}_2(\text{PO}_4)_2\text{F}_3/\text{C}$ Cathode in Sodium-Ion Batteries. *Sci. Bull.* **2020**, 65 (9), 702–710. <https://doi.org/10.1016/j.scib.2020.01.018>.

- (34) Jiang, Y.; Yang, Z.; Li, W.; Zeng, L.; Pan, F.; Wang, M.; Wei, X.; Hu, G.; Gu, L.; Yu, Y. Nanoconfined Carbon-Coated $\text{Na}_3\text{V}_2(\text{PO}_4)_3$ Particles in Mesoporous Carbon Enabling Ultralong Cycle Life for Sodium-Ion Batteries. *Adv. Energy Mater.* **2015**, *5* (10), 1402104. <https://doi.org/10.1002/aenm.201402104>.
- (35) Liu, S.; Wang, L.; Liu, J.; Zhou, M.; Nian, Q.; Feng, Y.; Tao, Z.; Shao, L. $\text{Na}_3\text{V}_2(\text{PO}_4)_2\text{F}_3$ -SWCNT: A High Voltage Cathode for Non-Aqueous and Aqueous Sodium-Ion Batteries. *J. Mater. Chem. A* **2019**, *7* (1), 248–256. <https://doi.org/10.1039/C8TA09194C>.
- (36) Liao, J.; Hu, Q.; He, X.; Mu, J.; Wang, J.; Chen, C. A Long Lifespan Potassium-Ion Full Battery Based on KVPO_4F Cathode and VPO_4 Anode. *J. Power Sources* **2020**, *451*, 227739. <https://doi.org/10.1016/j.jpowsour.2020.227739>.
- (37) Liao, J.; Hu, Q.; Mu, J.; He, X.; Wang, S.; Jiemin, D.; Chen, C. *In Situ* Carbon Coated Flower-like VPO_4 as an Anode Material for Potassium-Ion Batteries. *Chem. Commun.* **2019**, *55* (92), 13916–13919. <https://doi.org/10.1039/C9CC06948H>.
- (38) Petříček, V.; Dušek, M.; Palatinus, L. Crystallographic Computing System JANA2006: General Features. *Z. Für Krist. - Cryst. Mater.* **2014**, *229* (5). <https://doi.org/10.1515/zkri-2014-1737>.
- (39) Baur, W. H. The Geometry of Polyhedral Distortions. Predictive Relationships for the Phosphate Group. *Acta Crystallogr. B* **1974**, *30* (5), 1195–1215. <https://doi.org/10.1107/S0567740874004560>.
- (40) Bérar, J.-F.; Lelann, P. E.s.d.'s and Estimated Probable Error Obtained in Rietveld Refinements with Local Correlations. *J. Appl. Crystallogr.* **1991**, *24* (1), 1–5. <https://doi.org/10.1107/S0021889890008391>.
- (41) Shvets, P.; Dikaya, O.; Maksimova, K.; Goikhman, A. A Review of Raman Spectroscopy of Vanadium Oxides. *J. Raman Spectrosc.* **2019**, *50* (8), 1226–1244. <https://doi.org/10.1002/jrs.5616>.
- (42) Frost, R. L.; Scholz, R.; Lopes, A.; Xi, Y.; Gobac, Ž. Ž.; Horta, L. F. C. Raman and Infrared Spectroscopic Characterization of the Phosphate Mineral Paravauxite $\text{Fe}_2\text{Al}_2(\text{PO}_4)_2(\text{OH})_2 \cdot 8\text{H}_2\text{O}$. *Spectrochim. Acta. A. Mol. Biomol. Spectrosc.* **2013**, *116*, 491–496. <https://doi.org/10.1016/j.saa.2013.07.048>.
- (43) Merlen, A.; Buijnsters, J.; Pardanaud, C. A Guide to and Review of the Use of Multiwavelength Raman Spectroscopy for Characterizing Defective Aromatic Carbon Solids: From Graphene to Amorphous Carbons. *Coatings* **2017**, *7* (10), 153. <https://doi.org/10.3390/coatings7100153>.

- (44) Ferrari, A. C. Raman Spectroscopy of Graphene and Graphite: Disorder, Electron–Phonon Coupling, Doping and Nonadiabatic Effects. *Solid State Commun.* **2007**, *143* (1–2), 47–57. <https://doi.org/10.1016/j.ssc.2007.03.052>.
- (45) Buiel, E. R.; George, A. E.; Dahn, J. R. Model of Micropore Closure in Hard Carbon Prepared from Sucrose. *Carbon* **1999**, *37* (9), 1399–1407. [https://doi.org/10.1016/S0008-6223\(98\)00335-2](https://doi.org/10.1016/S0008-6223(98)00335-2).
- (46) Farivar, F.; Lay Yap, P.; Karunagaran, R. U.; Losic, D. Thermogravimetric Analysis (TGA) of Graphene Materials: Effect of Particle Size of Graphene, Graphene Oxide and Graphite on Thermal Parameters. *C* **2021**, *7* (2), 41. <https://doi.org/10.3390/c7020041>.
- (47) Maetz, A.; Delmotte, L.; Moussa, G.; Dentzer, J.; Knopf, S.; Ghimbeu, C. M. Facile and Sustainable Synthesis of Nitrogen-Doped Polymer and Carbon Porous Spheres. *Green Chem.* **2017**, *19* (9), 2266–2274. <https://doi.org/10.1039/C7GC00684E>.
- (48) Nita, C.; Fullenwarth, J.; Monconduit, L.; Le Meins, J.-M.; Fioux, P.; Parmentier, J.; Matei Ghimbeu, C. Eco-Friendly Synthesis of SiO₂ Nanoparticles Confined in Hard Carbon: A Promising Material with Unexpected Mechanism for Li-Ion Batteries. *Carbon* **2019**, *143*, 598–609. <https://doi.org/10.1016/j.carbon.2018.11.069>.
- (49) Matei Ghimbeu, C.; Zhang, B.; Martinez de Yuso, A.; Réty, B.; Tarascon, J.-M. Valorizing Low Cost and Renewable Lignin as Hard Carbon for Na-Ion Batteries: Impact of Lignin Grade. *Carbon* **2019**, *153*, 634–647. <https://doi.org/10.1016/j.carbon.2019.07.026>.
- (50) Bie, X.; Kubota, K.; Hosaka, T.; Chihara, K.; Komaba, S. A Novel K-Ion Battery: Hexacyanoferrate(II)/Graphite Cell. *J. Mater. Chem. A* **2017**, *5* (9), 4325–4330. <https://doi.org/10.1039/C7TA00220C>.